Chapter 5

H_2O and OH Gas in the Terrestrial Planet-Forming Zones of Protoplanetary Disks

This chapter, with minor differences, was published in its entirety with authors C. Salyk, K. M. Pontoppidan, G. A. Blake, F. Lahuis, E. F. van Dishoeck, and N. J. Evans II in *The Astrophysical Journal*, 2008, Volume 676, pp. L49–L52.

5.1 Abstract

We present detections of numerous 10–20 μm H_2O emission lines from two protoplanetary disks around the T Tauri stars AS 205A and DR Tau, obtained using the InfraRed Spectrograph on the Spitzer Space Telescope. Follow-up 3–5 μm Keck-NIRSPEC data confirm the presence of abundant water and spectrally resolve the lines. We also detect the P4.5 (2.934 μm) and P9.5 (3.179 μm) doublets of OH and $^{12}CO/^{13}CO$ v=1$\rightarrow$0 emission in both sources. Line shapes and LTE models suggest that the emission from all three molecules originates between $\sim$ 0.5 and 5 AU, and so will provide a new window for understanding the chemical environment during terrestrial planet formation. LTE models also imply significant columns of H_2O and OH in the inner disk atmospheres, suggesting physical transport of volatile ices either vertically or radially; while the significant radial extent of the emission stresses the importance of a more complete understanding of nonthermal excitation processes.

5.2 Introduction

One of the most intriguing questions in the study of the formation of planets, and of terrestrial planets in particular, is how water is transported to their surfaces, and whether or not water is a common ingredient during their formation and early evolution. Spatially and spectrally resolved observations of water in extrasolar planetary systems and protoplanetary disks would be instrumental in resolving these questions. Unfortunately, detecting water in extrasolar planetary systems remains difficult (Ehrenreich et al., 2007) and water in protoplanetary disks has been elusive, with only a few definitive ice (Malfait et al., 1998; Terada et al., 2007) and vapor (Carr et al., 2004) detections. Recently, however, the Spitzer InfraRed Spectrograph (IRS) has begun to reveal warm water vapor emission lines from disks around classical T Tauri stars (cTTs, Carr & Najita 2008).

In this chapter, we present high-resolution spectroscopy of numerous water vapor emission lines from protoplanetary disks around two cTTs: DR Tau and AS 205A. Spectra were obtained using both the Spitzer-IRS and NIRSPEC (McLean et al., 1998) at the Keck II telescope. Accretion rates onto these stars are high, which causes the inner disks to be significantly hotter than in more quiescent systems. DR Tau is known to have variable mass accretion, with measured rates between 0.3 and $79 \times 10^{-7}\,M_{\odot}\,\mathrm{yr}^{-1}$ (Gullbring et al., 2000; Johns-Krull and Gafford, 2002). AS 205A has an accretion rate of $7.2 \times 10^{-7}\,M_{\odot}\,\mathrm{yr}^{-1}$ and is the primary component of a 1.3" triple system, with the secondary being a spectroscopic binary (Eisner et al., 2005). However, it is likely that the physical separation of AS 205A and B is significantly larger than the projected separation and that, therefore, AS 205B does not affect the (inner) disk of AS 205A (Andrews and Williams, 2007a).

5.3 Observations

The Spitzer IRS Short-High (SH) module spectrum of AS 205A was taken as part of the "cores to disks" (c2d) legacy program (Evans et al., 2003; Kessler-Silacci et al., 2006), while the spectrum of DR Tau, observed as part of the guaranteed time observations (Houck et al., 2004), was obtained from the Spitzer archive. The 2-D basic calibrated data images were reduced using the c2d pipeline

as described in Lahuis and Kessler-Silacci (2006).

To confirm the detections as well as measure the gas emission line profiles, we obtained high resolution ($\lambda/\Delta\lambda$=25000) L-band spectra using NIRSPEC in a single grating setting, of which two orders, centered at 2.92 μm and 3.16 μm, respectively, have identifiable H_2O and OH emission features. We also collected CO v=1→0 M-band spectra ($\sim 5\,\mu$m) as part of an on-going survey (see Blake and Boogert, 2004; Salyk et al., 2007). The data were reduced in a standard way. Division by the spectra of standard stars (HR 1620 (A7V) for DR Tau; HR 5993 (B1V) for AS 205A) was used to correct for telluric absorption, which can be poor when the absorption is high. Thus, regions of the spectrum with $< 70\%$ atmospheric transmission were removed. Fluxes were calibrated using the photometry and spectral types of the standards, and are generally accurate to $\lesssim 20\%$.

The NIRSPEC lines are narrow (FWHM $\lesssim 35$ km s^{-1}), spatially unresolved, and centered at the stellar $v_{\rm LSR}$ (Herbig and Bell, 1988; Thi et al., 2001) to within our uncertainty (a few km s^{-1})—all consistent with disk emission. Because the disks are optically thick and heated from above, the line emission likely arises from the upper disk atmosphere (Najita et al., 2003).

5.4 Results

5.4.1 Spitzer-IRS

The IRS spectra of AS 205A and DR Tau show a large number of water emission lines (see Figure 5.1), the vast majority pure rotational transitions with quantum numbers in the range 20–50. The R=600 resolution of the SH module results in unresolved, and significantly blended, lines. Consequently, the identification with water is achieved via a simple, isothermal LTE ring model computed using the HITRAN 2004 database (Rothman et al., 2005). The ring model consists of a single temperature (T) and column density (N) gas in Keplerian rotation. Model parameters include T, N, solid angle (Ω), stellar mass ($M_\star$), inclination (i) and characteristic radius (r). In addition, the local line broadening is assumed to be Gaussian, with specified width (σ). $M_\star$ and i were fixed to values taken from the literature (Clarke and Bouvier, 2000; Kitamura et al., 2002; Eisner et al., 2005; Andrews and

Williams, 2007a). The spectrally unresolved IRS data cannot completely constrain the remaining model parameters, but do require high T ($T \gtrsim 500$ K) and N ($N \gtrsim 10^{17}$ cm^{-2} for $\sigma \sim 2$ km s^{-1}). Figure 5.1 compares the IRS spectra with a model in which T and N are constrained using the NIRSPEC data described below, but where Ω has been increased by a factor of 2.

The addition of CO_2 (and, for AS 205A, OH) improves our fits, as shown by the AS 205A model in Figure 5.1. With T and Ω fixed, we find H_2O:CO_2=40 for DR Tau and 20 for AS 205. Detections of these and other molecules will be discussed in detail elsewhere.

5.4.2 NIRSPEC

While tropospheric water vapor blocks significant portions of incoming radiation near 3 μm, there are a handful of rovibrational lines that are optically thin in the atmosphere but readily excited at temperatures typical of the inner $\sim$1 AU of circumstellar disks. This is illustrated in Figure 5.2, in which spectral regions with $< 70\%$ atmospheric transmission have been removed, yet many prominent (line-to-continuum $\sim$ 5–10%) H_2O emission features remain. These are primarily $\nu_3 = 1 \rightarrow 0$ lines, with upper level energies of $\sim$ 5,000–10,000 K. A few weaker (line-to-continuum $\sim$ 1%) features are nominally detected from 3.13–3.18 μm and are used as model constraints. We also detect the P4.5 (2.9344 μm; $T_{\rm up} \sim 5400$ K) and P9.5 (3.1788 μm; $T_{\rm up} \sim 7500$ K) OH doublets. The M-band spectra include portions of the ^{12}CO/^{13}CO v=1$\rightarrow$0 and ^{12}CO v=2$\rightarrow$1 P- and R-branches (Figure 5.3).

We fit all spectra with the ring models described in §5.4.1. Because the CO lines span a large range of excitation energies, across which they transition from optically thick to optically thin, N, T, and Ω can be determined uniquely. Also, a constraint on $N_{\rm CO}$ is provided by the ^{13}CO lines (assuming a ^{12}CO:^{13}CO ratio, here fixed at 77, see Blake and Boogert, 2004). Thus, we began by fitting the CO emission by comparison with an excitation diagram of the v=1$\rightarrow$0 transitions (Figure 5.3), as described in Salyk et al. (2007). For our nominal H_2O and OH fits, we then fixed Ω and T to the CO-derived values to determine N—a reasonable, though not ideal, assumption, given the similarity in line shapes (see Figure 5.3).

Our nominal ring model is shown in Figure 5.2, with best-fit parameters in Table 5.1, and uncer-

tainties of order $\Delta N \sim 30\%$, $\Delta T \sim 15\%$ and $\Delta\Omega \sim 10\%$. We have fixed $r = 3$ AU to roughly match the emission profiles since the lineshape does not affect the integrated flux; we discuss lineshapes below. Ω corresponds to areas of 0.2 and 0.4 AU^2 for DR Tau and AS 205, respectively, at distances of 140 and 120 pc. Uncertainties in the nominal H_2O and OH fits are linked to CO uncertainties, but if T is instead allowed to vary, the H_2O spectra are consistent with $T\sim$ 900–1200/900–1100 K for DR Tau/AS 205A and ranges in N of about 1 order of magnitude. For OH, we can only constrain $T \gtrsim$900 K.

The model results depend crucially on the assumed local line width (σ), which is unknown. For our nominal model, we have adopted $\sigma = 2\,\mathrm{km\ s^{-1}}$—the sound speed for H_2 at 1000 K. However, we have also tested values between $\sim$ 0.3 and 10 km s^{-1}. We find that the opacity needs to remain similar from fit to fit, so that a change in σ^2 requires a proportional change in N. To maintain the flux level, the total number of molecules must remain similar, so an increase in σ implies a decrease in Ω. Accordingly, the CO:H_2O ratio changes by no more than a factor of ~ 2 between models. (If T_{H_2O} is not fixed, however, this ratio may change.) In addition, T is only weakly affected by σ, since it is set by the overall shape of the spectrum, rather than by the absolute flux levels.

NIRSPEC spectrally resolves the molecular emission, allowing an investigation of the disk gas kinematics. In Figure 5.3 we compare the unblended H_2O transition at 2.931 μm with a CO line composite constructed from an average of all v=1→0 lines. In general, Keplerian disks should produce double-peaked emission profiles, with peak separation set by the inner and outer emission radii ($r_{\rm in}$, $r_{\rm out}$), as well as the temperature gradient (Horne and Marsh, 1986). The CO and H_2O line profiles, however, are more Gaussian, or even Lorentzian in shape, with relatively wide wings and a narrow peak. The narrow core could be produced by a ring with a very large $r_{\rm in}$ (>10 AU) if the peak-to-peak separation is equal to the NIRSPEC resolution (given the $M_\star$ and i in Table 5.1). However, this is difficult to reconcile with the high T derived from the model fits and the observed line wings.

Another way to produce a single peak would be to have the line emission extend to significant radii ($r_{\rm out}$ of order 7 AU, for a temperature profile that is constant with radius), such that the

contribution from low-velocity portions of the disk infills the center of the line profile. However, this model produces too much flux to match observations. Additionally, passive disk models predict a steep temperature decline with radius. A more promising solution may be that some flux is produced via fluorescence, in which molecules in the flared outer disk (typically out to ~ 5 AU) intercept and re-radiate inner disk IR continuum, thus filling in the line profiles at low velocity (Blake and Boogert, 2004). With canonical disk flaring and temperature structure, we find that a resonance fluorescence model with 100% scattering efficiency can indeed produce fluxes comparable to those of thermal emission; a more thorough investigation is left as future work.

In any case, the amount of flux in the line profile wings is consistent with emission arising in a Keplerian disk with a small inner radius. With this assumption, the line wing velocity can be used to estimate $r_{\rm in}$. Because turbulent motion and disk structure can both have non-negligible effects on the line shapes, we adopt here the velocity, $v_{\rm in}$, at 2.2 times the Half Width at Half Maximum—a value found to be appropriate for the moderate-inclination disk around GM Aur (Salyk et al., 2007). To compute $v_{\rm in}$ we use Gaussian fits to the CO and H_2O lines discussed above, as well as the average of two-Gaussian fits to the OH emission doublets, deconvolved with the NIRSPEC instrument response function. If turbulent velocities are low, radii associated with $v_{\rm in}$ will be overestimates, and so we also compute v at 3σ, which should represent a lower limit to $r_{\rm in}$ (see Table 5.1).

5.5 Discussion

We have convincingly detected H_2O emission in the 10–20 μm region with Spitzer-IRS as well as H_2O and OH emission near 3 μm with NIRSPEC, arising from the disk atmospheres surrounding two cTTs. By combining these data with constraints from spectrally resolved CO v=1→0 emission, we find that the excitation temperatures are typical of terrestrial planet-forming regions (~ 1000 K). Additionally, line wing velocities imply inner emission radii no larger than 1 AU for all molecules. Therefore, further observations and analyses of these species may provide a new window into terrestrial planet-forming regions.

Observations of H_2O in disks may also provide constraints on disk evolution and water transport.

In a disk in which water vapor transport is controlled by diffusion, the presence of a condensation front ('snow line') can potentially dry out an inner disk in as little as 10^5 yr, for typical disk viscosities (Stevenson and Lunine, 1988). The snow line for the early solar system is estimated to be near 3 AU, but would be further out for these high-accretion-rate stars (Lecar et al., 2006). Therefore, the presence of significant water vapor inside 1 AU may be evidence for inward radial migration, or upward mixing, of icy solids, followed by evaporation. With both solid migration and diffusion controlling water transport, water vapor concentrations become sensitive to an array of parameters, including disk viscosity and planetesimal growth rates, and water concentrations may trace disk evolution (Ciesla and Cuzzi, 2006).

The detection of strong OH emission is also interesting, for OH is known to be an important ingredient to the chemistry in the inner regions of protoplanetary disks. It also acts as a coolant near the disk surface (e.g., Dullemond et al., 2007), and photolysis of OH to O(^{1}D) has been invoked to explain the observed strengths of the 6300 Å O I line (Acke et al., 2005). Detections of OH in these and other disks will be discussed in greater detail in Mandell et al. (in prep).

An understanding of the local line broadening in disks will be crucial for obtaining accurate absolute column densities of molecular species, as smaller local line widths require lower column densities and vice versa. Nevertheless, we find that molecular ratios are more robust, and remain similar when utilizing different disk models, with the nominal fits having CO:H_2O $\sim$ 9–10 and H_2O:OH $\sim$ 3–4, provided $T_{H_2O} = T_{OH} = T_{CO}$. Stronger constraints on both T and N will require high line-to-continuum observations across a wider wavelength range, but the available data reveal that H_2O:CO is similar to, or slightly higher than that in the dense clouds out of which disks form (Boogert et al., 2004). Vertically integrated H_2O:OH ratios have been predicted to be much higher ($> 10^5$) near 1 AU (Markwick et al., 2002), but significant OH abundances are expected near the C^+/C/CO transition zone at large scale heights (Kamp and Dullemond, 2004). Also, it is important to keep in mind that disk transport is not included in current chemical models.

Our analysis of the L- and M-band spectra thus far has assumed thermal excitation of the vibrationally excited states, but this need not be the case. Δv=1 emission can also be driven by the

stellar UV output or by the absorption of IR photons from the star or disk, followed by fluorescence (dello Russo et al., 2004; Blake and Boogert, 2004). For OH, vibrationally excited emission can also result from the (photo)dissociation of H_2O followed by prompt emission (Bonev et al., 2006). In fact, fluorescence may be necessary to explain observed line profile shapes (see Section 5.4.2), and could explain the surprisingly strong OH emission. A better understanding of these processes may therefore prove essential for relating observed line fluxes to disk column densities.

If emission in the line wings truly represents emission from the disk inner radius, relatively large inner emission radii are implied for CO, OH, and H_2O. Both DR Tau and AS 205A have had their dust inner rim sizes measured with the Keck Interferometer. At 0.11 ± 0.03 and 0.07 ± 0.01 AU, respectively, they are consistent with the location of dust sublimation (Akeson et al., 2005b; Eisner et al., 2005), while the inner emission radii we derive are at least 3 times larger. Perhaps these high accretion-rate stars can stir up the inner disk enough to erase the vertical temperature gradients necessary for formation of emission lines. Another possibility may be that replenishment rates cannot keep up with photo-dissociation at the disk surface.

The ease with which H_2O and OH are now detected in the terrestrial planet-forming zones of certain disks holds the promise of more extensive and detailed studies. Although the ground-based echelle observations presented here probe only the inner disk atmospheres, future high-spectral-resolution follow-up studies of Spitzer-detected water emission from protoplanetary disks will provide constraints at a variety of disk radii and vertical depths. Additionally, spectro-astrometric observations are being used to directly constrain emitting location and structure of the molecular gas (Pontoppidan et al., 2008a). Eventually, a suite of constraints combined with non-LTE radiative transfer models will allow us to rigorously address such far-reaching questions as: How does the water vapor abundance vary within and between disks? What constraints can be put on models for the chemistry and transport of volatiles in disks, and what implications will these have for the early evolution of the Solar System?

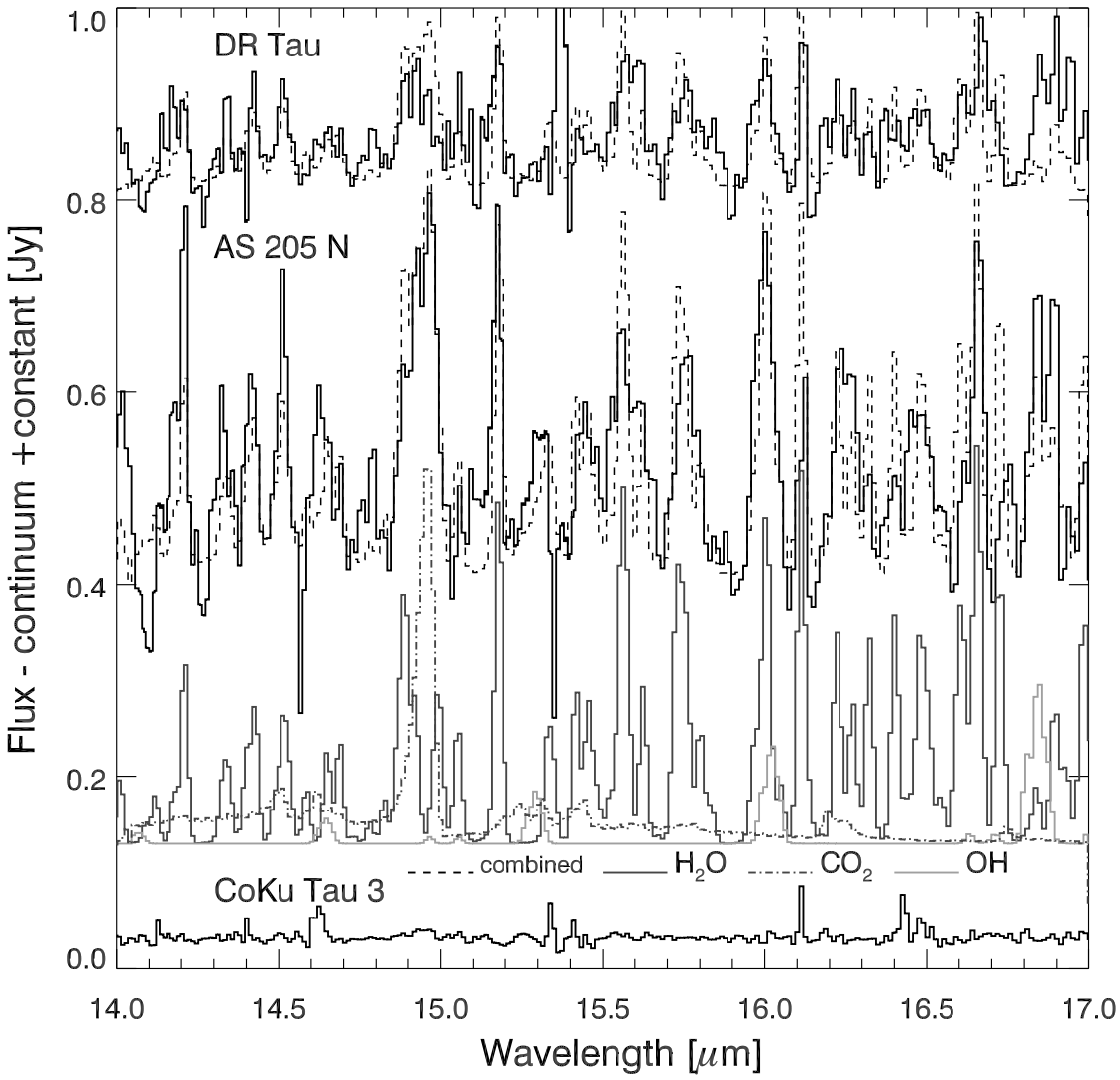

Figure 5.1: Spitzer-IRS spectra of DR Tau and AS 205 A. A portion of the Spitzer-IRS data (in black) and molecular emission models (dashed). The three components of the AS 205A model are shown below, in gray. The largely featureless spectrum of CoKu Tau/3 is included to demonstrate the dynamic range achievable by the IRS and the level of systematics, such as residuals from the de-fringing process. For both spectra, splines have been used to remove broad continuum features from silicates. Line-to-continuum excesses are $\sim$5–10%.

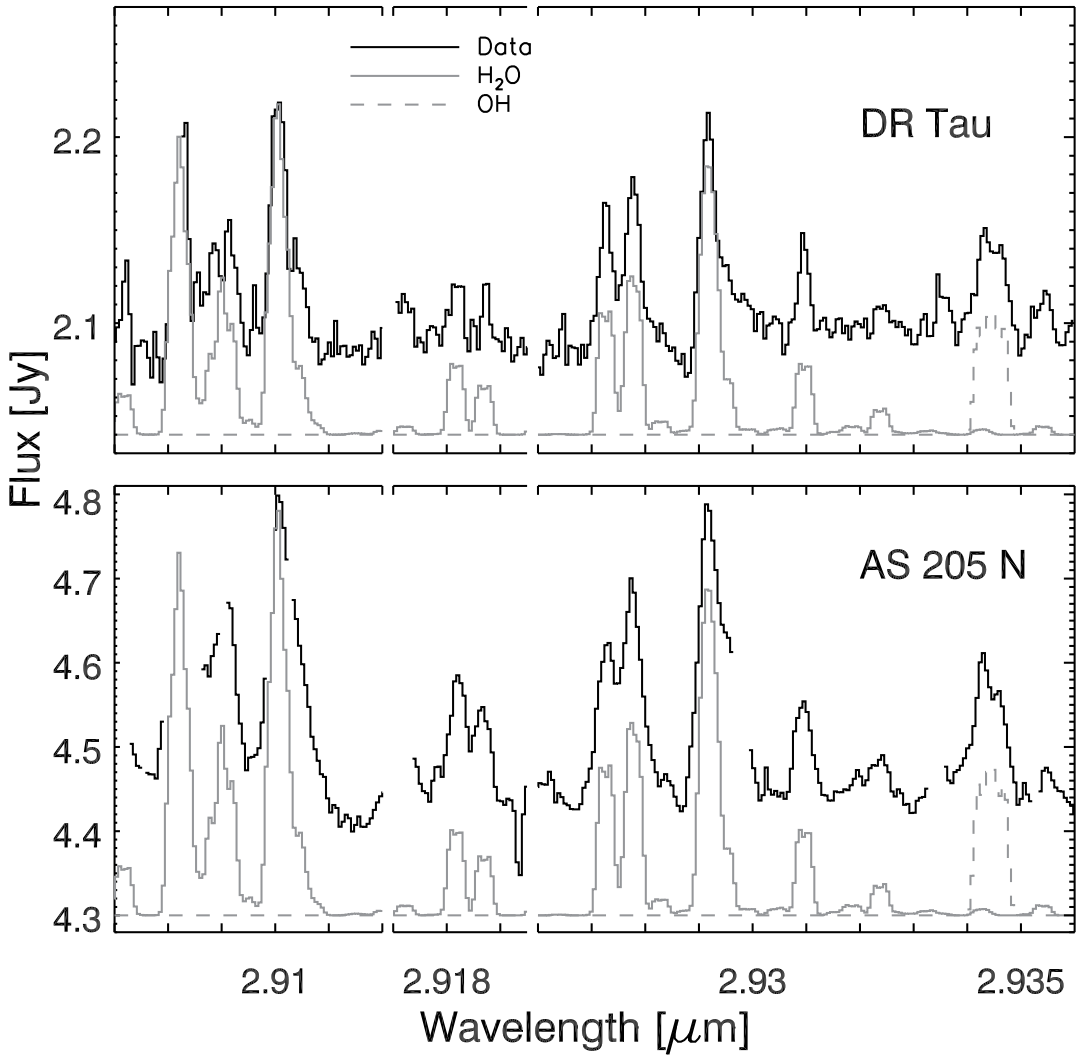

Figure 5.2: NIRSPEC L-band spectra of DR Tau and AS 205 A. Comparison between portions of the NIRSPEC L-band data and best-fit H_2O/OH disk models (offset).

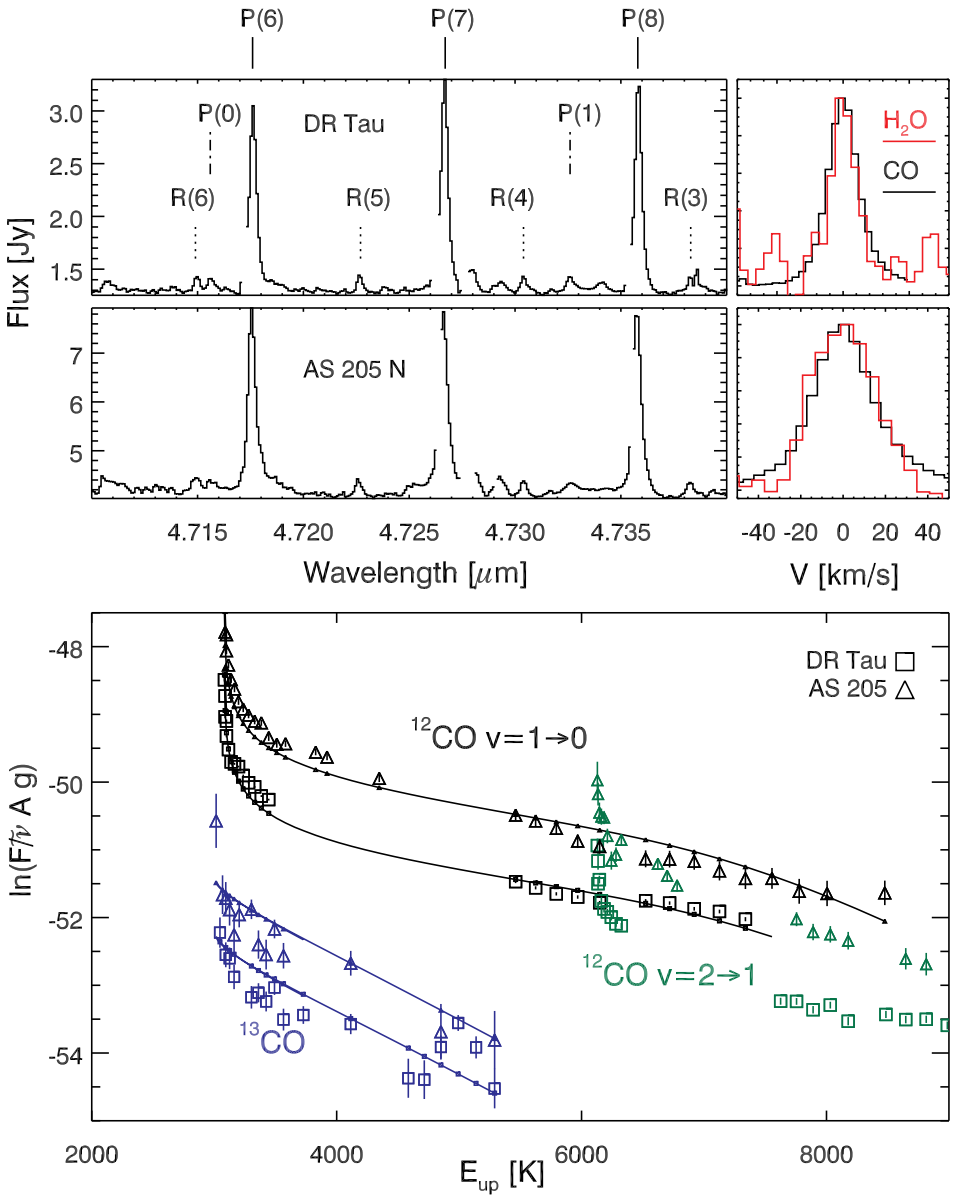

Figure 5.3: NIRSPEC CO emission spectra and rotation diagrams for DR Tau and AS 205 A. Top, left: a portion of the NIRSPEC M-band spectra. ^{12}CO/^{13}CO v=1→0 transitions are marked with solid and dashed lines, respectively. ^{12}CO v=2→1 transitions are marked with dot-dashed lines. Top, right: CO and H_2O emission lines are overplotted. Bottom: an excitation diagram with 1σ error bars and best-fit models to the v=1→0 transitions, with F in W m^{-2} and $\tilde{\nu}$ in cm^{-1}.

Table 5.1. Fits to NIRSPEC Data

	DR Tau	AS 205 A
CO $v_{\rm in}$, $v_{3\sigma}$ [km s^{-1}]	27, 32	35, 40
CO $r_{\rm in}$, $r_{3\sigma}$ [AU]	0.8, 0.6	0.5, 0.4
H_2O $v_{\rm in}$, $v_{3\sigma}$ [km s^{-1}]	24, 28	36, 42
H_2O $r_{\rm in}$, $r_{3\sigma}$ [AU]	1.0, 0.7	0.4, 0.3
OH $v_{\rm in}$, $v_{3\sigma}$ [km s^{-1}]	28, 32	34, 39
OH $r_{\rm in}$, $r_{3\sigma}$ [AU]	0.7, 0.5	0.5, 0.4
r[AU] [a]	3	3 [b]
σ [km s^{-1}] [a]	2	2
$M_\star$ [$M_\odot$] [a]	0.76	1.2
i[°] [a]	67	47
$\Omega_{\rm CO,H_2O,OH}$ [sr]	2×10^{-16}	6×10^{-16}
$T_{\rm CO,H_2O,OH}$ [K]	1000	1000
$N_{\rm CO}$ [cm^{-2}]	7×10^{18}	6×10^{18}
$N_{\rm H_2O}$ [cm^{-2}]	8×10^{17}	6×10^{17}
$N_{\rm OH}$ [cm^{-2}]	2×10^{17}	2×10^{17}

[a] Fixed

[b] Chosen to approximately match line shapes